Journal for ImmunoTherapy of Cancer

Combination of ultrasound-based mechanical disruption of tumor with immune checkpoint blockade modifies tumor microenvironment and augments systemic antitumor immunity

Shinya Abe,[1,2] Hiroshi Nagata,[1,2] Erika J Crosby ,[1] Yoshiyuki Inoue,[1,3] Kensuke Kaneko,[1,2] Cong-Xiao Liu,[1] Xiao Yang,[1] Tao Wang,[1] Chaitanya R Acharya ,[1] Pankaj Agarwal,[1] Joshua Snyder,[1] William Gwin,[4] Michael A Morse,[1,5] Pei Zhong,[6] Herbert Kim Lyerly ,[1] Takuya Osada [1]

To cite: Abe S, Nagata H, Crosby EJ, *et al*. Combination of ultrasound-based mechanical disruption of tumor with immune checkpoint blockade modifies tumor microenvironment and augments systemic antitumor immunity. *Journal for ImmunoTherapy of Cancer* 2022;**10**:e003717. doi:10.1136/jitc-2021-003717

► Additional supplemental material is published online only. To view, please visit the journal online (http://dx.doi.org/10.1136/jitc-2021-003717).

Accepted 13 December 2021

For numbered affiliations see end of article.

Correspondence to
Dr Takuya Osada;
osada001@duke.edu

ABSTRACT

Background Despite multimodal adjuvant management with radiotherapy, chemotherapy and hormonal therapies, most surgically resected primary breast cancers relapse or metastasize. A potential solution to late and distant recurrence is to augment systemic antitumor immunity, in part by appropriately presenting tumor antigens, but also by modulating the immunosuppressive tumor microenvironment (TME). We previously validated this concept in models of murine carcinoma treated with a novel predominately microcavitating version of high-intensity focused ultrasound (HIFU), mechanical high-intensity focused ultrasound (M-HIFU). Here we elucidated the mechanisms of enhanced antitumor immunity by M-HIFU over conventional thermal high-intensity focused ultrasound (T-HIFU) and investigated the potential of the combinatorial strategy with an immune checkpoint inhibitor, anti-PD-L1 antibody.

Methods The antitumor efficacy of treatments was investigated in syngeneic murine breast cancer models using triple-negative (E0771) or human ErbB-2 (HER2) expressing (MM3MG-HER2) tumors in C57BL/6 or BALB/c mice, respectively. Induction of systemic antitumor immunity by the treatments was tested using bilateral tumor implantation models. Flow cytometry, immunohistochemistry, and single-cell RNA sequencing were performed to elucidate detailed effects of HIFU treatments or combination treatment on TME, including the activation status of CD8 T cells and polarization of tumor-associated macrophages (TAMs).

Results More potent systemic antitumor immunity and tumor growth suppression were induced by M-HIFU compared with T-HIFU. Molecular characterization of the TME after M-HIFU by single-cell RNA sequencing demonstrated repolarization of TAM to the immunostimulatory M1 subtype compared with TME post-T-HIFU. Concurrent anti-PD-L1 antibody administration or depletion of $CD4^+$ T cells containing a population of regulatory T cells markedly increased T cell-mediated antitumor immunity and tumor growth suppression at distant, untreated tumor sites in M-HIFU treated mice compared with M-HIFU monotherapy. CD8 T and natural killer cells played major roles as effector cells in the combination treatment.

Conclusions Physical disruption of the TME by M-HIFU repolarizes TAM, enhances T-cell infiltration, and, when combined with anti-PD-L1 antibody, mediates superior systemic antitumor immune responses and distant tumor growth suppression. These findings suggest M-HIFU combined with anti-PD-L1 may be useful in reducing late recurrence or metastasis when applied to primary tumors.

BACKGROUND

Triple-negative and human ErbB-2 (HER2)-positive breast cancers (BCs) have a high rate of metastatic spread despite initial localized presentations and multimodality therapy.[1–3] Cancer immunotherapy in the form of immune checkpoint blockade (ICB) has had modest activity limited to small percentages of triple-negative BCs.[4 5] The reasons for the limited efficacy of ICB therapy in BC include a relatively low somatic mutation rate, the failure of the tumor to attract an immune infiltrate, particularly tumor-infiltrating lymphocytes, expression of additional immune checkpoint molecules in the tumor microenvironment (TME) suppressing the adaptive immune response,[6] and suppression of intratumoral innate immunity by inhibitory cell type, such as regulatory T cells (Tregs), tumor-associated macrophages (TAMs), and myeloid derived suppressor cells. In fact, aggressive BC growth and invasion have been associated with TAM in both preclinical and clinical studies.[7] Consequently, modifying the polarization of TAM in the TME has become a focus of attempts to

increase the efficacy of BC immunotherapy.[8] Unfortunately, pharmacological strategies to specifically modulate TAMs, without systemic alteration in non-TAM, have not been successful to date,[9] and alternatives such as local delivery or ablation are being pursued.[10–13]

Locally ablating tumor cells in the TME by image-guided delivery of various energies, including high-intensity focused ultrasound (HIFU), radiofrequency, microwaves, and cryoprobes has been clinically used as a minimally invasive therapy for localized prostate, breast, liver, kidney, bone and brain tumors.[14 15] Such ablative therapies produce tumor cell destruction using different sources of energy but also elicit antitumor immune response against antigens within the tumor debris in situ.[16 17] Conventional HIFU (thermal high-intensity focused ultrasound (T-HIFU)) induces rapid coagulative necrosis of the tissue at the targeted foci of applied energy.[18] Tissue proximal to the targeted foci, while not coagulated, undergoes thermal stress sufficient enough to cause apoptosis. As T-HIFU-treated cells release endogenous danger signals, resulting in secretion of interferon gamma (IFN-γ) and/or tumor necrosis factor alpha (TNF-α) from immune cells,[18 19] an increase in accumulation of $CD4^+$ and $CD8^+$ cells in T-HIFU-treated tumors has been observed.[20–23] Nonetheless, limitations to the efficacy of T-HIFU in larger tumors[24] have led to the study of alternative forms of HIFU to destroy tumors, such as high-pressure bursts that cause acoustic cavitation that we term mechanical high-intensity focused ultrasound (M-HIFU).[25] We have previously reported that, compared with T-HIFU, M-HIFU increased the accumulation of dendritic cells in treated tumors, demonstrated stronger antitumor efficacy, generated enhanced antitumor immunity, and reduced the risk of metastasis.[25 26] We noted that M-HIFU also increased the infiltration of T cells in the treated tumors.

To better delineate the mechanism for the greater antitumor immunity induced by M-HIFU, we used single-cell RNA sequencing of the tumor and TME following either no treatment or conventional T-HIFU and M-HIFU. We evaluated changes in the local and distant TMEs of murine BCs and observed a switch in macrophage subtype within M-HIFU-treated tumors that was absent following T-HIFU treatment. Further, we noted upregulation of immune checkpoint molecules, such as programmed cell death-1 (PD-1)/programmed cell death ligand 1 (PD-L1), lymphocyte activation gene 3 or TIM-3, which could exhaust activated T cells in the TME, resulting in the suppression of antitumor immunity.[21] Therefore, we studied the combination of M-HIFU and anti-PD-L1 therapy, which demonstrated upregulated gene expression by $CD8^+$ T cells in type I interferon-mediated signaling pathway, T-cell proliferation, and chemokine/cytokine secretion, and was associated with dramatic increases in the local and distant antitumor effects, including complete responses in the majority of treated animals.

METHODS

Cell lines

MM3MG, a murine premalignant mammary epithelial cell line, was transduced with the human HER2 oncogene by retroviral vectors and polybrene to express HER2 (referred to as MM3MG-HER2 cells) in our laboratory.[27] JC cells, a murine BC cell line, were transduced with human HER3 gene (referred to as JC-HER3) in our laboratory.[28] 4T1-HER2 cells were obtained from Dr Michael Kershaw (Peter MacCallum Cancer Center, Victoria, Australia).[29]

HIFU procedure

The VIFU 2000 system (Alpinion Medical Systems, Bothell, Washington, USA) was used for HIFU treatment. Cells or tumors were treated using a 1.5 MHz HIFU transducer under two different protocols (50% duty cycle, 1 Hz pulse repetition frequency, 20 W, 10 s or 2% duty cycle, 5 Hz pulse repetition frequency, 200W, 20 s) to produce either thermal necrosis or mechanical lysis of the tumor cells. The former was defined as T-HIFU, and the latter was defined as M-HIFU.[30] T-HIFU increased the temperature inside tumor tissues to >60°C in a few seconds, while the temperature inside tumor tissue was <42°C during M-HIFU. M-HIFU is similar to boiling histotripsy,[31] which produces cavitation activities in vivo that may damage tumor tissue and cells through shear stresses generated by the complex bubble oscillation and bubble–bubble–tissue–cell interactions.[32] The −6 dB focal dimension of the HIFU transducer was measured at a low-power level of 10 W to be 0.72 mm×7.22 mm in the lateral and axial directions, respectively. At the high-power levels used for T-HIFU (20 W) and M-HIFU (200 W), the corresponding focal dimensions based on numerical simulations were estimated to be 0.74 mm×6.50 mm and 0.60 mm×5.69 mm, respectively (see online supplemental methods). Concerning focus for the treatment, both X and Y axis intervals were 2 mm, and a total of 9 points were selected in both in vitro and in vivo studies. A shorter interval of 1 mm was used only when tumors did not have enough size to put 2 mm for all intervals. The same spacing strategy was used for both M-HIFU and T-HIFU. To avoid skin or bone damage by HIFU treatment, tumor tissue just beneath the skin or close to thighbone was spared from exposure of focused ultrasound; thus, approximately 20%–40% of tumor tissues were ablated by HIFU treatments based on macroscopic assessment.

Mice

Female BALB/c mice or SCID-beige mice 5–8 weeks old (Jackson Labs, Bar Harbor, Maine, USA) were bred and maintained in the Duke Cancer Center Isolation Facility. Human HER2-transgenic mice were a kind gifted by Dr Wei-Zen Wei (Wayne State University, Detroit, Michigan, USA).[33] F1 hybrid HER2 transgenic mice were established by crossing with BALB/c mice. Human HER3-transgenic mice (MMTV–neu/

MMTV-hHER3) with FVB background were a kind gift from Dr Stan Gerson at Case Western Reserve University.[6] FVB mice homozygous for the hHER3 gene were established at Duke University and then crossed with BALB/c mice for establishment of BALB/c homozygous for the hHER3 gene.

Animal studies

All animal studies were performed in accordance with Duke Institutional Animal Care and Use Committee-approved protocols. Mice were euthanized when the local tumor volume reached 2000 mm^3. To test the immunogenicity of HIFU-treated tumor cells, BALB/c mice received intradermal injections of in vitro T-HIFU-treated or M-HIFU-treated MM3MG-HER2 cells (1×10^6 cells) into the back on days −14 and −7. On day 0, some mice were euthanized and spleen, draining lymph nodes, and blood were collected for in vitro assays: IFN-γ ELISpot, flow cytometry, and cell-based ELISA. Other mice (10 mice/group) were inoculated with 1×10^6 MM3MG-HER2 cells into the left leg. Tumor size was measured serially and tumor volumes were calculated using the formula long axis×(short axis)^2×0.5.

For the therapeutic models using MM3MG-HER2 tumors, MM3MG-HER2 cells were subcutaneously inoculated into the left leg (1×10^6 cells) of the mice on day 0. In the bilateral tumor model, 1×10^5 or 5×10^5 cells were also inoculated into the right flank on day 0. Established leg tumors were treated with T-HIFU or M-HIFU on day 7. For the rechallenge experiment, mice cured by M-HIFU treatment received a subcutaneous injection of MM3MG-HER2 cells (1×10^6 cells) into the flank on day 35 (28 days after M-HIFU) and tumor size and mouse survival were monitored. For the combination treatment with anti-PD-L1 antibody, mice received peritoneal injection of 100 µg anti-PD-L1 antibody (clone 10F.9G2, Bio X Cell, West Lebanon, NH) or Isotype control IgG (clone LTF-22, Bio X Cell) on days 12, 15 and 18 in unilateral tumor models, or on days 10, 13 and 16 in bilateral tumor models. For JC-HER3 tumor model, cells were inoculated into the left leg (1×10^6 cells)±inoculation into the right flank (5×10^5 cells) on day 0. Leg tumors were treated with M-HIFU on day 8 (for combination treatment experiments) or 11 (for single M-HIFU treatment experiments). For the combination treatment, mice received intraperitoneal injection of anti-PD-L1 antibody or Isotype control IgG (200 µg/injection) on days 8, 11, 15 in unilateral tumor models, or on days 8, 11, 15 and 18 in bilateral tumor models. For depletion of immune cells, mice received peritoneal injection of 250 µg antibody against CD4 (clone GK1.5, Bio X Cell), against CD8a (clone 53–6.72, Bio X Cell) or 10 µL antibody against natural killer (NK) cells (anti-Asialo GM1 antibody; Wako Pure Chemical Corporation, Osaka, Japan) 1 day before the first HIFU treatment and 2 days after the first HIFU treatment, followed by injection of the same amount every 5 days throughout experiments.

IFN-γ ELISpot assay

Mouse IFNγ- ELISpot assays (Mabtech, Cincinnati, Ohio, USA) were performed according to the manufacturer's instructions. Cells were stimulated with HER2 intracellular domain (ICD) peptide, HER2 extracellular domain (ECD) peptide (25 µg/mL; JPT Peptide Technologies, Berlin, Germany) or irrelevant HIV-gag peptide mix (2.6 µg/mL, JPT Peptide Technologies). The number of IFN-γ spots was counted with a high-resolution automated ELISpot reader system (Carl Zeiss, White Plains, New York, USA) using the KS ELISpot V.4.2 software.

Cell-based ELISA

Plates were coated with 3×10^4 4T1 parental cells or 6×10^4 4T1-HER2 cells per well overnight. A serial dilution of serum (final titrations 1:50–1:6400) was added, incubated for 1 hour on ice. The plates were washed and fixed with 1% formalin, followed by incubation with IRDye 800CW Donkey anti-mouse (1:2000; LI-COR Biosciences, Lincoln, Nebraska, USA) for 60 min. Fluorescence intensity was determined using an Odyssey CLx LI-COR reader (LI-COR) using the 800 nm channel.

ELISA

Tumors were weighed and homogenized in Cell Lysis Buffer (Cat#9803, Cell Signaling, 9 times volume of tumor weight) with added PMSF (1 mM) using Qiagen TissueRupter (Qiagen, Germantown, Maryland, USA) for up to 20 s on ice. Tumor homogenates were then sonicated using Branson Ultrasonic SLPe Digital Sonifier Cell Disruptor (Branson Ultrasonics, Danbury, Connecticut, USA) for 10 s on ice. Sonicated samples were centrifuged at 13 000 rpm at 4°C for 20 min, and collected supernatants were used as tumor lysates for ELISAs.

Tumor lysates were assessed for the level of IFN-γ, TNF-α and transforming growth factor beta 1 (TGF-β1) using commercially available ELISA kits for IFN-γ (Cat#ab46081; Abcam, Cambridge, Massachusetts, USA), TNF-α (BMS607-3; Invitrogen, Waltham, Massachusetts, USA) and TGF-β1 (BMS608-4, Invitrogen), and assays were performed according to the manufacturers' instructions.

Flow cytometry

Single-cell suspensions of tumor tissue were obtained by manually disrupting tumor using a razor followed by enzymatic digestion. Single-cell suspensions of spleen and lymph nodes were obtained by manual mashing and filtration through a 70 µm cell strainer (BD Biosciences, San Jose, California, USA). Cell were stained using LIVE/DEAD Fixable Aqua Dead Cell Stain Kit (Thermo Fisher Scientific, Rockford, Illinois, USA), then stained with surface marker antibody (online supplemental table 1) for 30 min, at room temperature. Isotype IgG or fluorescence minus one (FMO) controls were used as negative staining controls. Anti-CD16-32 antibody (Thermo Fisher) was used to block FcγIII/II receptor. Intracellular staining was carried out using Fixation/Permeabilization

and Permeabilization Buffer (Thermo Fisher) following the manufacturer's instructions. Stained cells were acquired on an LSRII flow cytometer (BD Biosciences) and analyzed using FlowJo software IX (BD Biosciences).

Single-cell RNA sequencing and analysis

Single-cell suspensions dissociated from untreated or HIFU treated tumor (8 days after HIFU treatment) were obtained as described above . For combination therapy experiments, mice received intraperitoneal injections of 100 µg anti-PD-L1 antibody or isotype control IgG antibody both 3 and 6 days after HIFU treatment. $CD45^+$ leukocytes were sorted from the tumor digest by flow cytometry, and a cDNA library was prepared using Bio-Rad single-cell isolator (ddSEQ) and SureCell WTA 3'Library Prep kits from Illumina. Raw sequencing data was generated in the form of FastQ files which were uploaded to a BaseSpace sequencing Hub (Illumina, San Diego, California, USA) for expression quantification using an automated pipeline. The resulting gene expression matrix files for each treatment condition were analyzed using Partek Flow software (Partek, St. Louis, Missouri, USA). Unsupervised clustering was done to separate the cell types and markers for the cell types were identified using differential gene expression. These markers were then used for identifying the cell subpopulations within the $CD45^+$ sorted immune cells.[7 8] The preprocessed gene counts were used to generate Uniform Manifold Approximation and Projection (UMAPs) for visualization of the cell types in different treatment conditions. Gene Ontology (GO) enrichment analysis, Kyoto Encyclopedia of Genes and Genomes (KEGG) pathway analysis, and differential gene expression analysis were done using Partek Flow software.

Immunohistochemistry staining

Staining of formalin-fixed paraffin-embedded tumor tissue sections was performed using rabbit–anti-mouse CD3ε antibody (1:150, D4V8L; Cell Signaling Technology, Danvers, Massachusetts, USA), CD4 antibody (1:100, D7D2Z; Cell Signaling) or CD8a antibody (1:400, D4W2Z; Cell Signaling) by the horseradish peroxidase (HRP) method. Antigen retrieval was performed with Citrate Unmasking Solution (Cell Signaling). Before incubation with HRP (Histofine Simple Stain Mouse MAX PO (R), Nichirei Biosciences, Tokyo, Japan), DAB Substrate Kit (Vector Labs, Burlingame, California, USA) was used for visualization of signal. Isotype-matched rabbit IgG was used as a negative staining control. Stained slides were scanned on a DP80 microscope (OLYMPUS, Tokyo, Japan) and digital images were viewed using cellSens (OLYMPUS).

Statistical analysis

Data are presented as mean±SEM in tumor growth graphs, or as mean±SD for in vitro assays and flow cytometry data. Tumor volumes, flow cytometry, ELISA, and ELISPOT data from experiments with three or more treatment groups were analyzed by one-way analysis of variance with Tukey's multiple comparisons test. A two-tailed, unpaired Student's t-test was used for experiments with only two groups. Tumor volumes were analyzed at the terminal endpoint only, unless otherwise indicated. Statistical analyses were performed using Prism (GraphPad, San Diego, California, USA). Kaplan-Meier survival curves for tumor-bearing mice were generated and log-rank tests were performed using JMP Pro V.11.0 software (SAS Institute, Cary, North Carolina, USA). P values of 0.05 or less were considered statistically significant. Not all significant differences are shown in every graph (*p<0.05, **p<0.01, ***p<0.001).

RESULTS

M-HIFU elicits stronger systemic cellular antitumor immunity than T-HIFU

We treated implanted MM3MG-HER2 BCs in BALB/c mice with either M-HIFU or T-HIFU and assessed the antitumor effect on both the local (treated) and distant tumor mass. There was greater control of the treated tumors as well as untreated distant tumors with M-HIFU compared with T-HIFU (figure 1A–C). Tumor growth suppression of both the treated and untreated disease sites by M-HIFU was confirmed in two other murine BC models, E0771-OVA and JC-HER3 (online supplemental figure 1). M-HIFU could induce significantly stronger cellular immune responses for HER2 ECD, HER2 ICD and mixed peptide antigens when compared with untreated control, while T-HIFU could induce only mildly stronger response for HER2 ECD antigen (figure 1D). There was a clear trend for stronger cellular immune responses induced by M-HIFU compared with T-HIFU. However, M-HIFU and T-HIFU induced similar levels of humoral immunity against HER2 expressing tumor cells (figure 1E). Also in JC-HER3 tumor model, we could confirm the induction of HER3 antigen-specific cellular immune response in HER3 transgenic mice after M-HIFU treatment, suggesting the strong capacity of M-HIFU for the induction of antitumor immunity by breaking tolerance (online supplemental figure 2). Importantly, there was a long-lived immune memory response induced in mice that had previously rejected their tumor following M-HIFU treatment (figure 1F). This memory response could not be measured in T-HIFU-treated mice as none of the treated tumors fully regressed (figure 1B).

A potential explanation for this difference in antitumor response is a baseline difference in the immunogenicity of tumor cells following treatment with M-HIFU compared with T-HIFU. To test this hypothesis, we vaccinated mice with in vitro HIFU-treated MM3MG-HER2 cells and assessed their immunogenicity. Despite a difference in the type of cell death induced by M-HIFU versus T-HIFU (apoptosis vs necrosis; online supplemental figure S3A,B), there was no significant difference in the systemic T-cell activation (online supplemental figure 3C,D), generation of tumor antigen-specific antibodies (online supplemental figure S3E), or tumor control

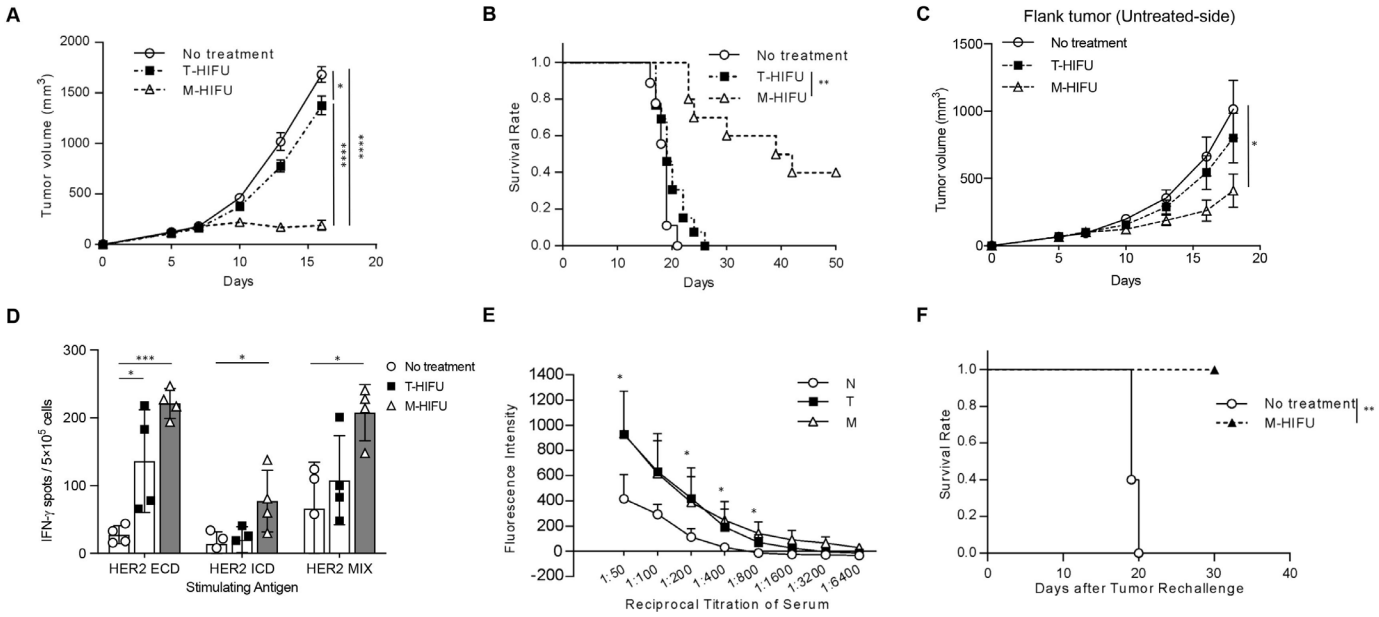

Figure 1 Superior growth suppression of local and distant tumors and enhanced tumor antigen-specific cellular immune responses by M-HIFU compared with T-HIFU. (A) 1×10^6 MM3MG-HER2 cells were injected into the legs of BALB/c mice. Established leg tumors were treated with M-HIFU or T-HIFU on day 7 after tumor inoculation. Comparison of tumor growth curves is shown. (B) Survival curves are shown. Mice were euthanized when tumor volume reached 2000 mm^3 or on day 50. n=9 mice (no treatment), 10 (M-HIFU) or 13 (T-HIFU) (A,B), 32 mice in total. Log-rank test was performed. (C) MM3MG-HER2 cells were injected into the left leg (1×10^6 cells) and the right flank (1×10^5 cells) of the HER2 transgenic mice on day 0. Leg tumors were treated with M-HIFU or T-HIFU on day 7. Comparison of flank tumor growth curves is shown. n=13 mice (no treatment) or 14 (M-HIFU and T-HIFU), 41 mice in total. (D) Lymphocytes were isolated from the spleen on day 18 after tumor inoculation (11 days after HIFU treatment), and IFN-γ secretion was detected by an ELISpot assay. Average values of spot numbers for HER2 peptide of ECD, ICD and mix (ECD+ICD) are shown. n=4 per group. (E) Serum was collected from mice on day 11 after HIFU treatment. The levels of anti-HER2 antibody in the serum of mice were evaluated with cell-based ELISA. n=3 mice (no treatment) or 8 (M-HIFU and T-HIFU), 19 mice in total. (F) Mice cured from MM3MG-HER2 tumor by M-HIFU treatment were rechallenged with subcutaneous injection of MM3MG-HER2 cells (1×10^6 cells/mouse) 28 days after M-HIFU treatment. Age-matched naive female BALB/c mice were used as a control group. The survival rate of mice is shown and log-rank test was performed. n=5 mice per group, 10 mice in total. (A–C) Error bars represent SE. (D,E) Error bars represent SD. *P<0.05, **P<0.01, ***P<0.001, ****P<0.0001. ECD, extracellular domain; HER2, human ErbB-2; ICD, intracellular domain, IFN-γ, interferon gamma; M-HIFU, mechanical high-intensity focused ultrasound; T-HIFU, thermal high-intensity focused ultrasound.

(online supplemental figure S3F) elicited by inoculation with M-HIFU or T-HIFU killed tumor cells.

Different modification of TME by M-HIFU compared with T-HIFU

Because tumor cells treated in vitro with M-HIFU or T-HIFU were similarly immunogenic, we hypothesized that differential modification of the TME by the two HIFU treatments was the cause of differences in the induction of systemic antitumor immunity, and thus efficacy, in our BC models. We observed greater CD4 and CD8 T-cell infiltration in M-HIFU-treated tumors and slightly increased T-cell infiltration in T-HIFU-treated tumors compared with no treatment controls by immunohistochemistry (figure 2A). This was confirmed by flow cytometry of digested tumors which demonstrated an increase in both CD4 and CD8 T cells as well as NK cells following M-HIFU treatment (figure 2). To confirm the modification of immune cell profile, absolute numbers of tumor-infiltrating immune cells were determined for each treatment group and shown in online supplemental figure 4. Increased numbers of CD4 T cells, CD8 T cells, and NK cells were confirmed in M-HIFU-treated tumors, while the differences in granulocytes and macrophage populations were not observed. Enhanced proliferation of T cells was seen in M-HIFU-treated tumors compared with control tumors by Ki67 staining (figure 2C). In addition to an increase in infiltration and active proliferation, the CD8 T cells present in M-HIFU-treated tumors had increased expression of T-cell activation markers and granzyme (figure 2D). In M-HIFU-treated tumors, dendritic cell (DC) maturation was increased as evidenced by upregulation of Major Histocompatibility Complex (MHC) class II and CD80 (figure 2E). Importantly, M-HIFU affected the polarization status of tumor-infiltrating macrophages as shown in figure 2F. Positivity of CD206 expression was significantly lower and expression level of MHC class II was significantly higher in macrophages in M-HIFU-treated tumors compared with those in control tumors, suggesting that M-HIFU can induce repolarization of macrophages and make more antitumor-TME. To support this finding, significantly lower TGF-β1 levels and higher IFN-γ levels were observed

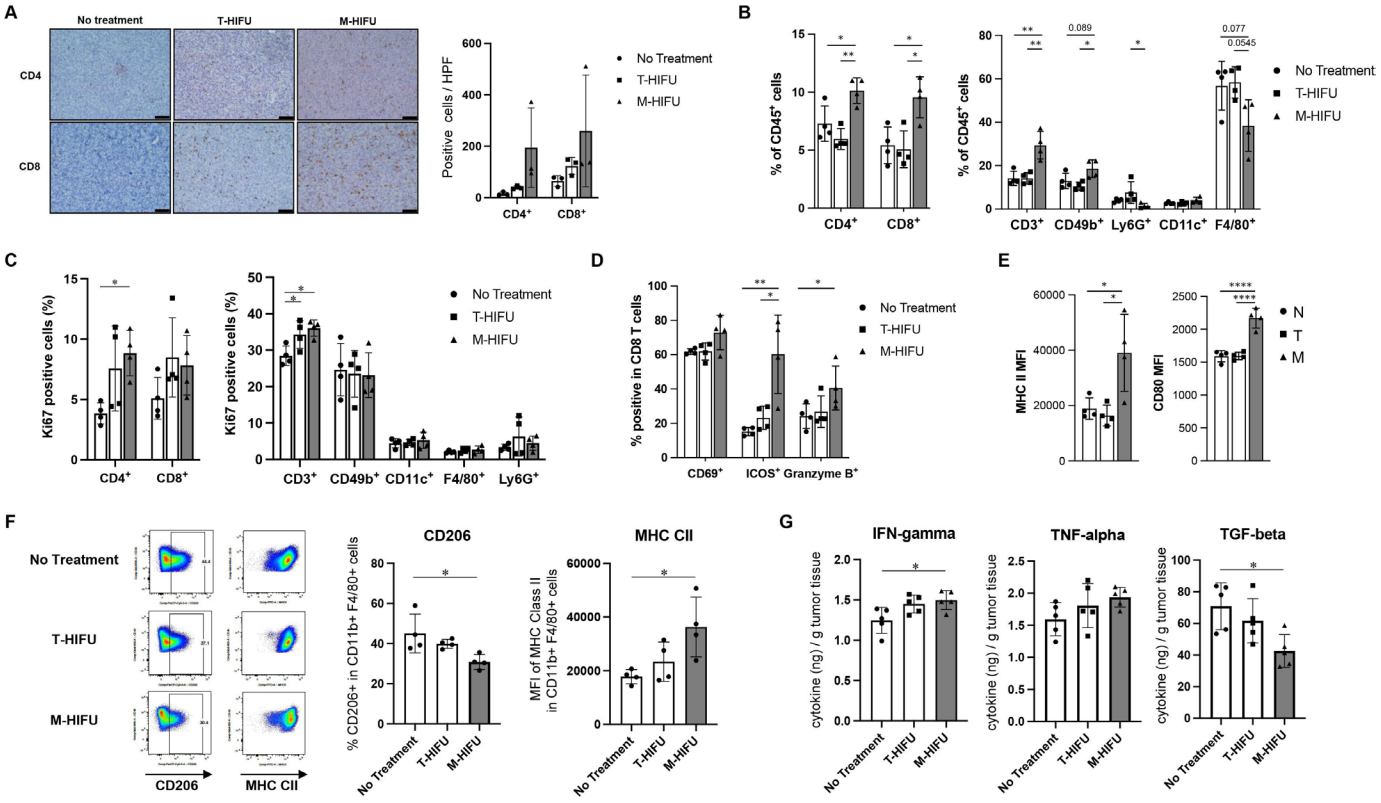

Figure 2 Enhanced intratumoral infiltration of activated CD4$^+$ and CD8$^+$ cells and M1 polarized macrophages by M-HIFU. 1×10^6 MM3MG-HER2 cells were injected into legs of BALB/c mice. Established leg tumors were treated with M-HIFU or T-HIFU on day 7 after tumor inoculation. (A) Immunohistochemical staining of T cells in tumor sections. Tumors on day 13 after HIFU treatment were collected, fixed with formalin and stained with anti-mouse CD4 and CD8 monoclonal antibodies. Representative images are shown (left: no treatment, middle: T-HIFU, right: M-HIFU). Scale bar is 50 µm. Quantification of positive cells in high-power field (HPF) is shown in the right panel. Error bars represent SD, n=3 per group. (B) Seven days after HIFU treatments of MM3MG-HER2 tumors in mice, tumors were collected and digested for flow cytometry analysis. The percentages of CD4$^+$, CD8$^+$, CD3$^+$, CD49b$^+$, Ly6G$^+$, CD11c$^+$, and F4/80$^+$ cells in alive CD45$^+$ cells were analyzed for each HIFU treatment group. n=4 per group. (C) The expression of proliferation marker Ki67 was analyzed for each cell type in tumor-infiltrating immune cells by flow cytometry, and percentages of Ki67 positive for each cell type are shown. n=4 per group. (D) The expression of CD69$^+$, Inducible T-cell costimulator (ICOS)$^+$, and granzyme B$^+$ by CD8$^+$ cells were analyzed by flow cytometry and shown for each HIFU treatment group. n=4 per group. (E) MFI of MHC class II (left) and CD80 (right) expression on CD11c$^+$ dendritic cells are shown for each HIFU treatment group. (F) Expression of CD206 and MHC class II by CD11b$^+$F4/80$^+$ macrophage population was analyzed for each treatment group. Representative dot plots of CD206 and MHC class II staining are shown in the left panel. Percentages of CD206-positive macrophages and mean fluorescence intensity of MHC class II expression are shown. n=4 per group. (G) ELISAs for IFN-γ, TNF-α, and TGF-β1 were performed with tumor lysates made from MM3MG-HER2 tumors treated with no treatment, T-HIFU or M-HIFU. n=5 per group. Error bars represent SD. *P<0.05, **P<0.01, ****P<0.0001. IFN-γ, interferon gamma; MFI, mean fluorescent intensity; M-HIFU, mechanical high-intensity focused ultrasound; TGF-β1, transforming growth factor beta 1; T-HIFU, thermal high-intensity focused ultrasound; TNF-α, tumor necrosis factor alpha.

in M-HIFU-treated tumors compared with control tumors (figure 2G).

To study the effect of HIFU on the TME in a more detailed fashion, we conducted single-cell RNA sequencing (scRNA-seq) analysis on tumor-infiltrating leukocytes from untreated tumors to compare with the gene expression from tumors treated with M-HIFU and T-HIFU (online supplemental figure 5). We performed GO enrichment analysis and KEGG pathway analysis of differentially expressed genes (DEGs) within the identified macrophage populations from the two HIFU strategies compared with macrophages in the untreated tumors. Ten of the significantly upregulated GO terms of the biological process category in M-HIFU-treated macrophages are shown in figure 3A. Upregulated genes were mainly involved in immune response, inflammatory response, leukocyte activation, immune system process, cell chemotaxis, endocytosis and regulation of apoptotic signaling pathway. A similar analysis of the top 10 differently expressed GO terms in T-HIFU-treated tumors did not contain any immune-related terms but rather centered around biosynthetic processes (online supplemental figure 6A).

The top 10 GO terms of the cellular components and molecular function categories for both M-HIFU-treated and T-HIFU-treated tumors compared with untreated tumors are shown in figure 3B,C, and online supplemental figure 6B,C, respectively. There is no overlap in the

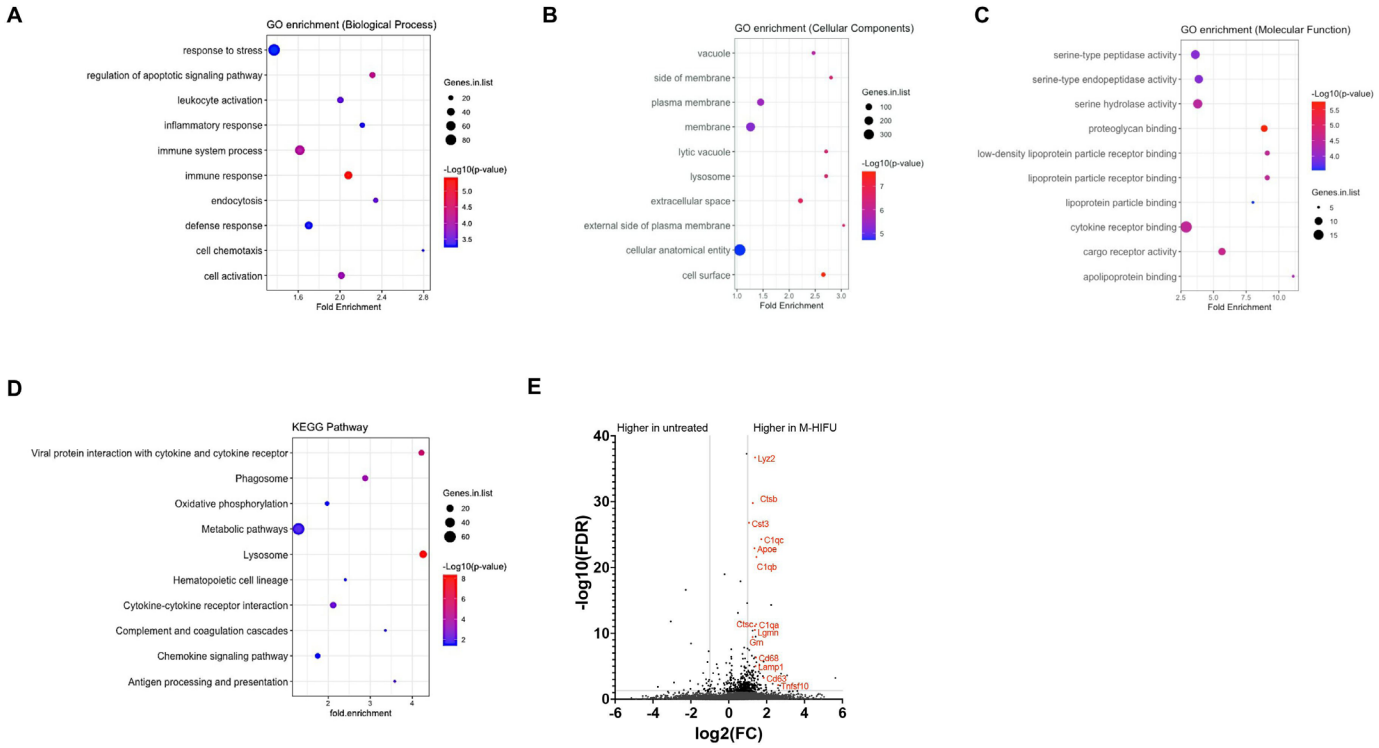

Figure 3 GO enrichment analysis and KEGG pathway analysis of DEGs in macrophages after M-HIFU treatment. (A–C) GO enrichment analysis of DEGs that are upregulated in macrophages derived from M-HIFU-treated tumors compared with macrophages from untreated tumors. Enrichment scores of GO terms are shown for the categories of (A) biological process, (B) cellular components, and (C) molecular function. (D) KEGG pathway analysis of DEGs that are upregulated in macrophages derived from M-HIFU-treated tumors compared with macrophages from untreated tumors. Top 10 KEGG pathways in terms of enrichment scores are demonstrated. (E) Differential gene expression analysis in tumor-infiltrating macrophages from M-HIFU-treated tumors compared to those from untreated tumors. Representative genes that were significantly upregulated in macrophages from the M-HIFU-treated group (log_2(fold Change)>1, FDR<0.05) are shown in red. DEG, differentially expressed gene; FDR, false discovery rate; GO, Gene Ontology; M-HIFU, mechanical high-intensity focused ultrasound.

top terms that are upregulated following these different forms of HIFU, again demonstrating fundamental differences in the molecular consequences of each therapy.

KEGG pathway analysis of M-HIFU-treated tumors shows that the top 10 upregulated pathways are enriched for antigen processing/presentation, cytokine–cytokine receptor interaction, chemokine signaling pathways, and phagosome/lysosome pathways, consistent with an inflammatory, antitumor phenotype of macrophages after M-HIFU (figure 3D). Tumors treated with T-HIFU only had seven KEGG pathways that were significantly upregulated compared with untreated tumors. These pathways were all involved in metabolic processes (online supplemental figure 3D). The differences in significantly upregulated pathways between M-HIFU-treated and T-HIFU-treated tumors highlight the immunogenic nature of our M-HIFU therapy at this timepoint.

Differential gene expression analysis of tumor-infiltrating macrophages identified 298 genes that were expressed at statistically higher levels (FDR adjusted p value <0.05) than untreated tumors (figure 3E). A number of genes (*Irg1*, *Ccl2*, *Maff*, *Ier3*, *Lcp2*, *Ptpn2*, *Cd14*, *Cxcl16*, *Ier3*, *Nfkbia*, *Ccrl2*, and *Tlr2*) are signature genes for M1/classically activated macrophages,[34] and other genes (*Tnfsf10Ctsc*, *Gzme*, *Cd8a*, and *Pdcd1*) are commonly associated with M1 macrophages.[35 36] These findings confirm a highly activated M1-biased macrophage population within the TME of M-HIFU-treated tumors. Thus, scRNA-seq analysis demonstrated that M-HIFU induced an inflammatory, M1-biased macrophage population, which might be contributing to the enhanced antitumor immunity in M-HIFU-treated tumors.

Increased expression of immune checkpoint molecules on tumor-infiltrating immune cells following M-HIFU

Despite productive antitumor immune responses in nearly half of M-HIFU-treated mice, many eventually developed progressive disease (figure 1A,B). We therefore investigated the etiology for this tumor escape, beginning by evaluating the expression of immune checkpoint molecules in M-HIFU-treated versus T-HIFU-treated tumors. At 7 days post-treatment, PD-L1 expression was increased on neutrophils ($Ly6G^+$), DCs ($CD11c^+$), and macrophages ($F4/80^+$) only in M-HIFU-treated tumors (figure 4A,B). Analysis at just 3 days after HIFU treatment, however, revealed that neither mode of HIFU treatment increased the PD-L1 expression in these tumor-associated cell populations (online supplemental figure 7). This suggests that HIFU itself does not cause immediate upregulation of PD-L1, but is instead the result of the ongoing immune

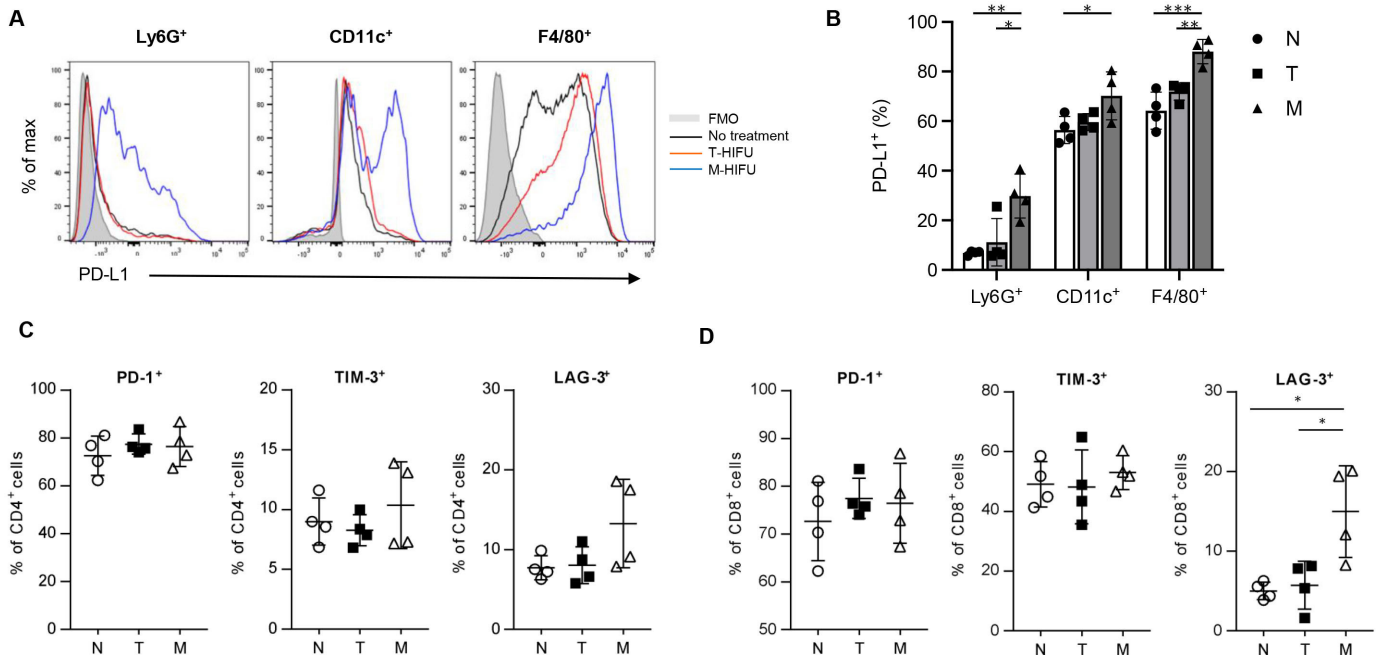

Figure 4 Enhanced expression of immune checkpoint molecules by tumor-infiltrating immune cells after M-HIFU treatment. (A) Representative flow cytometry histograms showing PD-L1 expression on Ly6G$^+$ cells, CD11c$^+$ cells and F4/80$^+$ cells are shown. Blue: M-HIFU, red: T-HIFU, black: no treatment, gray filled: isotype control. (B) Percentages of PD-L1$^+$ cells in Ly6G$^+$ cells, CD11c$^+$ cells, and F4/80$^+$ cells among alive CD45$^+$ tumor-infiltrating immune cells are shown for each HIFU treatment group. n=4 per group. (C, D) Expression of immune checkpoint molecules, PD-1, TIM-3 and LAG-3, on tumor-infiltrating CD4$^+$ (C) and CD8$^+$ (D) cells are shown. n=4 per group. Error bars represent SD. *P<0.05, **P<0.01, ***P<0.001. LAG-3, lymphocyte activation gene 3; M-HIFU, mechanical high-intensity focused ultrasound; PD-1, programmed death-1; PD-L1, programmed cell death ligand 1; T-HIFU, thermal high-intensity focused ultrasound.

response caused by M-HIFU treatment. IFN-γ, which was increased in tumor tissues on day 5 after M-HIFU treatment (figure 2G), might be playing an important role in this upregulation of PD-L1. Other immune checkpoint molecules including PD-1 and TIM3 were not significantly altered following M-HIFU, but lymphocyte activation gene 3 (LAG-3) expression on CD8$^+$ cells was significantly higher after M-HIFU than T-HIFU (figure 4C,D). Taken together, these data demonstrate enhanced antitumor immunity within the TME caused by M-HIFU that is not seen with T-HIFU but may be stifled by a concomitant increase in immune checkpoint molecules.

PD-1/PD-L1 blockade enhances the treatment efficacy of M-HIFU

Based on the upregulation of immune checkpoint molecules after M-HIFU, we hypothesized that PD-1/PD-L1 blockade could enhance the antitumor efficacy of M-HIFU treatment. To test this, M-HIFU treatment was combined with anti-PD-L1 antibody administration. This combined treatment cured 72.2% of mice implanted with MM3MG-HER2 tumors compared with 26.3% and 52.6% when anti-PD-L1 or M-HIFU, respectively, were given alone (figure 5A,B). The combination also resulted in tumor eradication and long-term survival in 37.5% of mice using another BC model, JC-HER3 (online supplemental figure 8). Analysis of IFN-γ ELISpot assay of splenocytes demonstrate a significant increase in the number of HER2-specific IFN-γ-secreting cells in mice treated with M-HIFU+anti-PD-L1 compared with those treated with M-HIFU or anti-PD-L1 alone (figure 5C). Flow cytometric analysis of digested tumors revealed that the proportion of CD4$^+$ T cells, CD8$^+$ T cells, and NK cells increased in tumors treated with combination therapy (figure 5D), and enhanced activation of both CD4$^+$ and CD8$^+$ T cells in combination therapy (online supplemental figure 9A,B). Stronger cytolytic activity of tumor-infiltrating CD8$^+$ T cells was suggested in M-HIFU monotherapy and combination therapy based on enhanced granzyme B expression (online supplemental figure 9B). Additionally, CD4$^+$Foxp3$^+$ Treg cells were increased in tumors treated with combination therapy compared with control tumors or tumors treated with M-HIFU monotherapy, although the difference was not statistically significant (online supplemental figure 9C).

In order to demonstrate which infiltrating cells were responsible for the observed antitumor efficacy, MM3MG-HER2 tumors were treated with combination therapy in the presence of depleting antibodies against CD4$^+$, CD8$^+$, or NK cells. Depletion of CD8$^+$ or NK cells abrogated the antitumor efficacy of the combination therapy, but depletion of CD4$^+$ cells did not result in appreciable change in antitumor effect (figure 5E,F).

Combination of M-HIFU and anti-PD-L1 treatment further activated CD8 T cells in the TME

In order to explain the enhanced antitumor efficacy of the addition of anti-PD-L1 treatment, we further

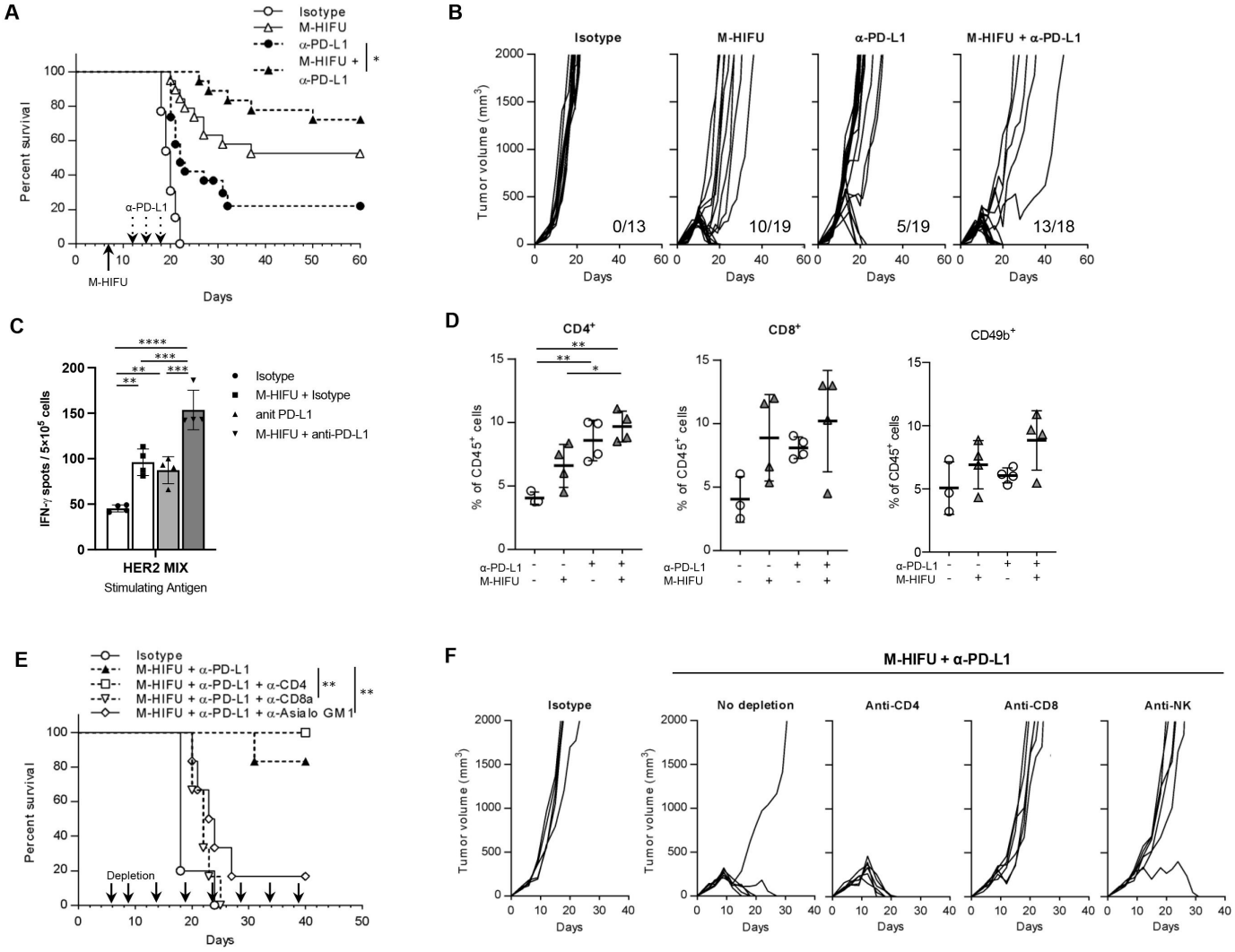

Figure 5 M-HIFU and PD-L1 blockade synergize to reject local tumor. (A) Established MM3MG-HER2 tumors in the legs of BALB/c mice were treated with M-HIFU on day 7. Anti-PD-L1 antibody (100 µg /100 µL) or isotype control IgG (100 µg/100 µL) was injected intraperitoneally 5, 8, and 11 days after M-HIFU treatment. Survival curves are shown and log-rank test was performed. n=13 mice (isotype control), 19 (monotherapy groups) or 18 (combination group), 50 mice in total. (B) Individual tumor growth curves are shown for each treatment group. The numbers in each plot show mice with tumor eradication/mice in the group. (C) Nine days after the initiation of M-HIFU treatment with/without anti-PD-L1 antibody, spleens were collected for immune assays. Induction of HER2 antigen-specific cellular response was analyzed by IFN-γ ELISpot assay using harvested splenocytes and HER2 peptide mix as a stimulating antigen. n=4 per each group. (D) The percentages of $CD4^+$, $CD8^+$, and $CD49b^+$ cells in tumor-infiltrating $CD45^+$ cells were analyzed by flow cytometry analysis. n=4 (treatment groups) or 3 (control group). (E,F) Mice were treated with the combination of M-HIFU and anti-PD-L1 antibody as in figure 4A, with or without administration of depleting antibody for $CD4^+$, $CD8a^+$ and NK cells on days 6, 9, 14, and every 5 days until the end of the experiment. n=5 mice (isotype control) or 6 (other groups), 29 mice in total. (E) Survival curves are shown and log-rank test was performed. (F) Individual tumor growth curves are shown for each cell depletion group. (C,D) Error bars represent SD. *P<0.05, **P<0.01, ***P<0.001, ****P<0.0001. HER2, human ErbB-2; IFN-γ, interferon gamma; M-HIFU, mechanical high-intensity focused ultrasound; PD-L1, programmed cell death ligand 1.

characterized leukocyte populations by conducting scRNAseq analysis on the tumor-infiltrating $CD45^+$ immune cells derived from mice treated with no treatment, M-HIFU, a-PD-L1 alone or combination treatment (figure 6). DEGs that were significantly upregulated in treatment groups compared with no treatment control were identified in CD8 T cells or macrophages, and the number of DEGs is shown in figure 6. In CD8 T cells, 1690 DEGs were identified in the three treated groups, and 333 genes among them were unique to the combination treatment, while 231 genes and 365 genes were unique to M-HIFU and anti-PD-L1 monotherapy, respectively, indicating that the combination treatment exerts not a mere additive effect of monotherapies (figure 6A).

The most significantly enriched GO terms of the upregulated DEGs in the combination treatment were shown as enrichment scores in the heatmap with other two treatments (figure 6B). In CD8 T cells, the DEGs mainly enriched in type I interferon-mediated signaling pathway, activated T-cell proliferation, chemokine

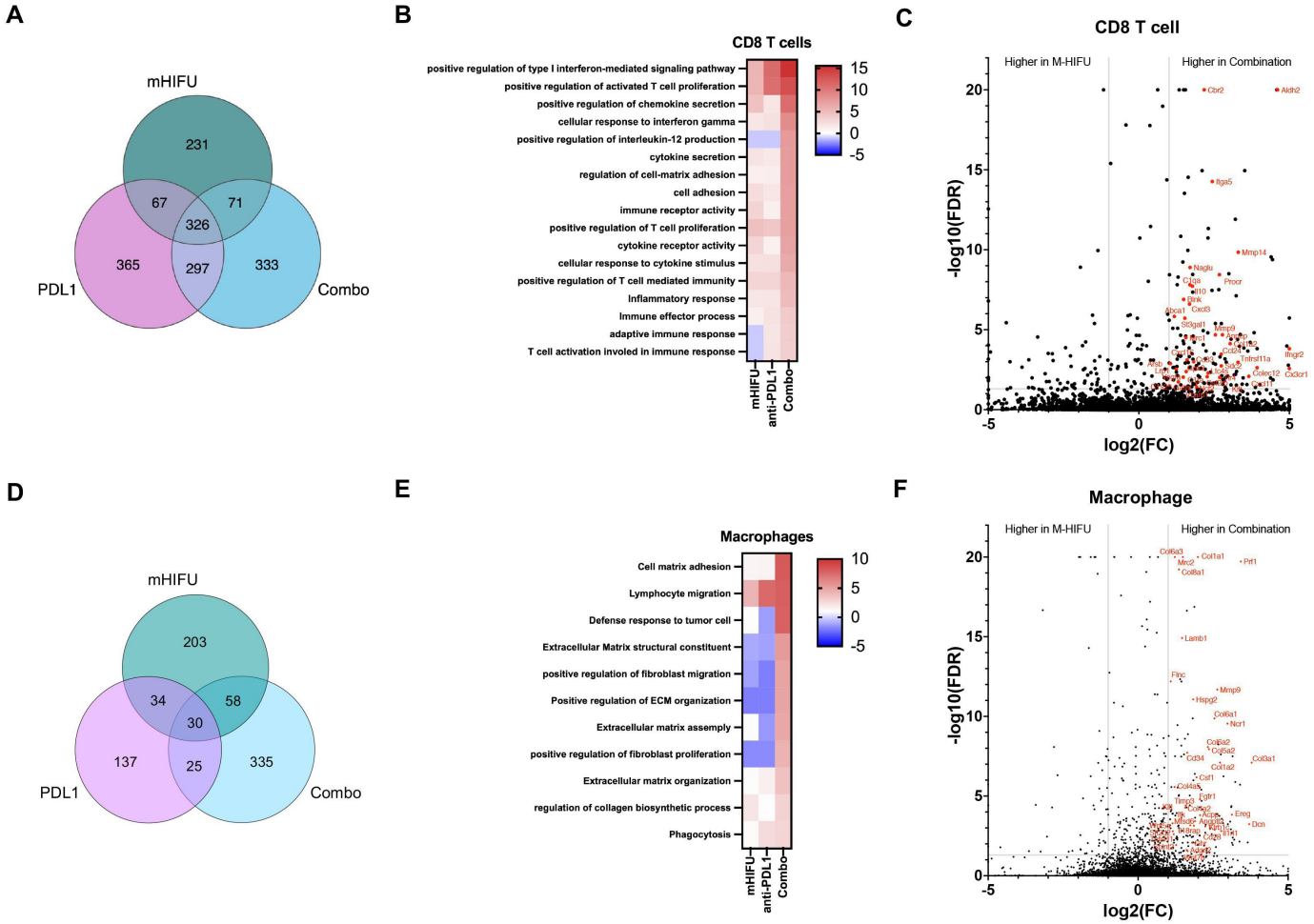

Figure 6 Combination of M-HIFU and anti-PD-L1 antibody induces upregulation of unique DEGs in tumor-infiltrating CD8 T cells and macrophages. Established MM3MG-HER2 tumors in the legs of BALB/c mice were treated with M-HIFU, followed by intraperitoneal injections of 100 µg anti-PD-L1 antibody or isotype control IgG antibody both 3 and 6 days after HIFU treatment. Alive CD45$^+$ leukocytes were isolated from enzymatically digested tumors by flow-based sorting and used for scRNA-seq. Data analysis was performed using Partek Flow software. (A) The numbers of DEGs of CD8 T cells that were upregulated in treatment groups compared with no treatment control are shown in the Venn diagram. (B) GO enrichment analysis was performed for the upregulated DEGs in CD8 T cells in each treatment group and summarized in the heatmap. Top 17 GO terms in combination treatment are shown together with enrichment data in M-HIFU and anti-PD-L1 monotherapy group. (C) Differential gene expression analysis was performed for upregulated DEGs in CD8 T cells between combination treatment and M-HIFU monotherapy. Representative DEGs that are significantly upregulated ($\log_2$(fold change)>1, FDR<0.05) in the combination group are shown in red letters. (D) The numbers of DEGs of macrophages that were upregulated in the treatment groups compared with no treatment control are shown in the Venn diagram. (E) GO enrichment analysis was performed for the upregulated DEGs in macrophages in each treatment group and summarized in the heatmap. Top 11 GO terms in the combination treatment are shown together with enrichment data in the M-HIFU and anti-PD-L1 monotherapy group. (F) Differential gene expression analysis was performed for upregulated DEGs in macrophages between combination treatment and M-HIFU monotherapy. Representative DEGs that are significantly upregulated ($\log_2$(fold change)>1, FDR<0.05) in the combination group and contributed to the activated KEGG pathways (online supplemental figure 7) or are known as M1 or M2 signature genes are shown in red letters. DEG, differentially expressed gene; GO, Gene Ontology; M-HIFU, mechanical high-intensity focused ultrasound; PD-L1, programmed cell death ligand 1.

secretion, cellular response to interferon gamma, interleukin (IL)-12 production, and cytokine secretion. KEGG pathway analysis indicates that upregulated DEGs were significantly enriched in pathways such as complement and coagulation cascades, cytokine–cytokine receptor interaction, and NF-kappa B signaling pathway (online supplemental figure 10A). Thus, the combination treatment appears to activate CD8 T cells through regulation of multiple pathways and enhance antitumor immunity.

To clarify the genes involved in enhanced antitumor efficacy of combination treatment over M-HIFU monotherapy, gene expression levels by CD8 T cells in the combination treatment and M-HIFU monotherapy were compared (figure 6C). Genes related to CD8 T-cell activation, such as *Cd33*, *Cx3cr1*, *Cxcl3*, *Cxcl11*, and *Cxcl16* were expressed more than twofold stronger following the combination treatment compared with M-HIFU monotherapy, confirming the enhanced activation of CD8 T cells by combining anti-PD-L1

to M-HIFU treatment, which corresponded to the superior antitumor efficacy against remote tumors observed in our bilateral tumor models.

In macrophages, among 822 DEGs significantly upregulated in the treated samples, 335 genes were unique to the combination treatment (figure 6D), mainly enriched in lymphocyte migration and defense response to tumor cells, as well as in the multiple pathways related to extracellular matrix/fibroblasts (figure 6E). KEGG pathway analysis revealed gene enrichment in protein digestion and absorption, extracellular matrix–receptor interaction, cell adhesion molecules, PI3K-Akt signaling pathway and T-cell receptor signaling pathway in the combination treatment (online supplemental figure 10B). These results may suggest more active involvement of combination therapy-treated macrophages in the enhanced antitumor activity and remodeling of tissues after disruption of tumors by ultrasound.

Interestingly, as shown in figure 6F, tumor infiltrating macrophages of the combination treatment group, when compared with those in M-HIFU treated tumors, showed relatively upregulated expression of genes signatures for both M1/classically activated macrophages (*Dcn*, *Acpp*, *Csf1*, *Adgrl2*, and *Col4a2*) and M2/alternatively activated macrophages (*Il1rl1*, *Mmp9*, *Mfsd6*, *Angptl2*, *Spint2*, and *Sft2d2*).[34]

Systemic PD-1/PD-L1 blockade enhances CD8 and NK cell-mediated antitumor immunity against distant tumors following local M-HIFU

Based on the enhancement of systemic tumor antigen-specific immune responses by the addition of anti-PD-L1 (figure 5C), we hypothesized PD-1/PD-L1 blockade would also improve the abscopal effect of M-HIFU. When we treated MM3MG-HER2 tumors with M-HIFU and administered intraperitoneal anti-PD-L1 antibody (figure 7A), we observed greater growth suppression against distant untreated tumors than with either treatment alone in a more stringent bilateral tumor model, where mice were implanted with a larger number of tumor cells (five times larger compared with figure 1C) to the flank (figure 7B).

To elucidate the change of TME in distant HIFU-untreated tumors induced by the combination treatment, distant tumors were analyzed by flow cytometry. As shown in figure 7C, M-HIFU monotherapy could not increase CD4 T/CD8 T/NK-cell infiltration in rapidly growing distant tumors, which might be the main reason for weaker antitumor effect on distant tumors. However, combination treatment as well as anti-PD-L1 monotherapy increased the proportion of $CD4^+$, $CD8^+$, and NK-cell populations in distant tumors, compared with the untreated control and M-HIFU monotherapy (figure 7C). Likewise, CD4 T cells again expressed higher levels of activation markers in these groups and granzyme B expression in CD8 T cells was significantly higher in distant tumors in the combination treatment group (figure 7D), suggesting the most enhanced cytotoxic function of CD8 T cells in combination group which lead to the strongest abscopal effect (figure 7B). Finally, to confirm which immune cells were responsible for the efficacy against the distant tumor in the bilateral tumor model, the mice were treated with M-HIFU+anti-PD-L1 therapy in the presence of depleting antibody for $CD4^+$, $CD8^+$, or NK cells (figure 7E). In both leg and flank tumors, depletion of $CD8^+$ or NK cells significantly abrogated the antitumor efficacy (figure 7F). Greater efficacy of the combination therapy against distant tumors in $CD8^+$ cell-dependent fashion was confirmed also in the JC-HER3 tumor model (online supplemental figure 11). To clarify how depletion of immune cells affect TME of the distant tumors in mice treated with the combination therapy, we analyzed the profile of tumor-infiltrating immune cells in distant tumors by flow cytometry (online supplemental figure 12). Interestingly, systemic depletion of $CD8^+$ or NK cells resulted in an intratumoral immune cell profile following M-HIFU+anti-PD-L1 that was similar to the profile of untreated control tumors (online supplemental figure 12A) and reduced ICOS expression and granzyme B production by CD8 T cells (online supplemental figure 12B), suggesting that these two cell types not only are the key effectors but may also influence the immune composition of the TME. On the other hand, depletion of $CD4^+$ cells induced significant increase and activation of CD8 T cells, and the decrease of macrophages and Treg in distant tumors (online supplemental figure 12A–C), that may explain the stronger abscopal effect observed in the $CD4^+$ depleted group. These results indicate that both $CD8^+$ cells and NK cells play significant roles in the immune-based attack of distant tumors as well as HIFU-treated tumors in this M-HIFU+anti-PD-L1 combination therapy.

DISCUSSION

Many approaches seeking to modify the TME to induce systemic antitumor immunity are under development,[37] including intratumoral delivery of cytokines and oncolytic viruses, and physical tumor destruction using, among others, focused ultrasound.[12 13] The traditional focused ultrasound approach creates coagulation necrosis by heating tissue (T-HIFU); however, it may not optimally induce systemic antitumor immunity due to denaturation of tumor proteins. Indeed, we previously reported that conventional T-HIFU modifies the TME, yet does not induce a memory systemic immune response.[30] Therefore, we studied M-HIFU, which causes cell death and extracellular matrix disruption by acoustic microcavitation rather than heating the tissue, and which we previously observed to improve antigen presentation, resulting in more favorable immune responses.[30]

In our current study, we demonstrate that M-HIFU induces local and systemic immunity against BC, that in our models is more potent than T-HIFU. This was evidenced by greater antigen presentation, induction of antigen specific T cells within splenocytes, and increased T cell infiltration at the site of M-HIFU-ablated as well as

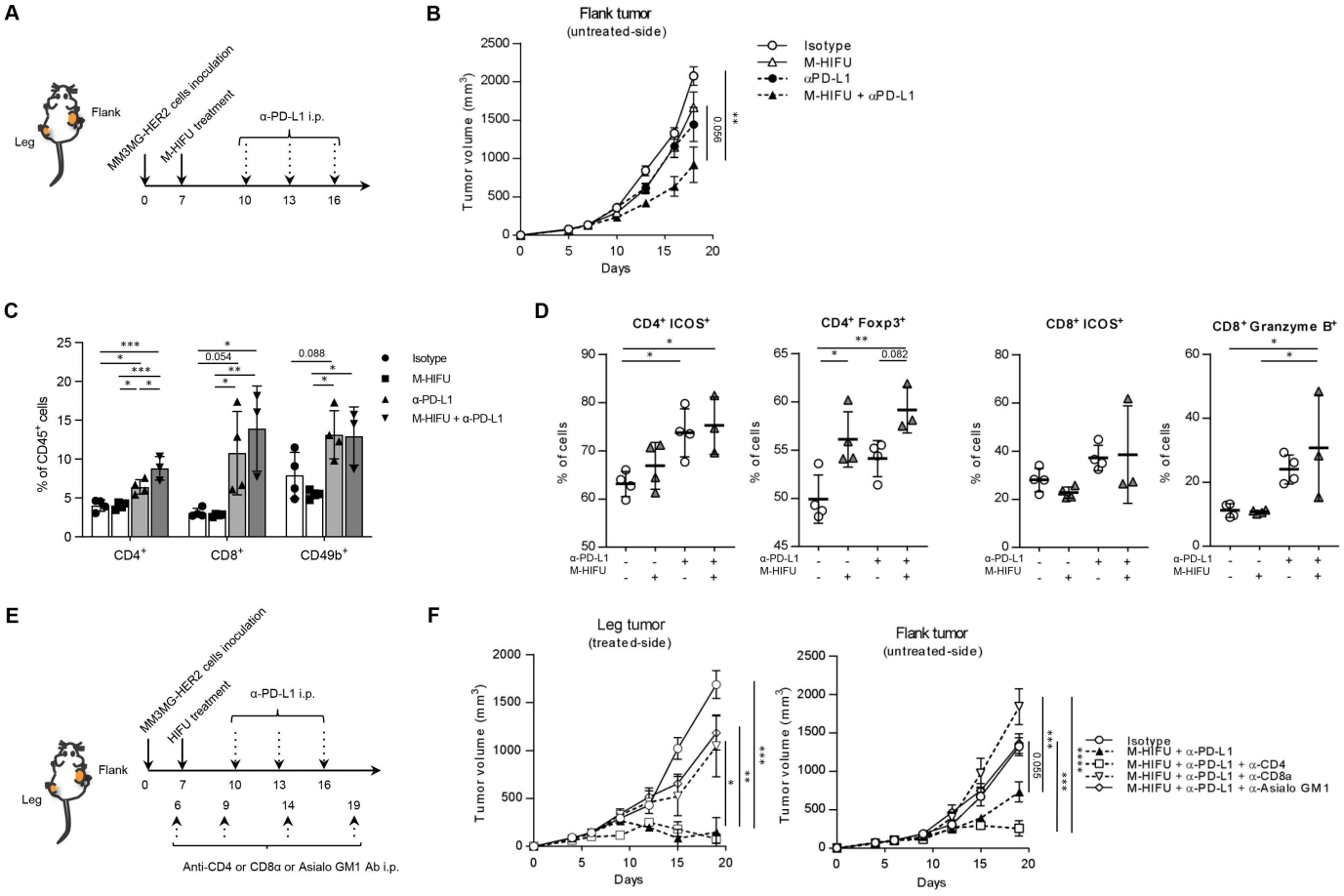

Figure 7 The combination of M-HIFU and PD-1/PD-L1 blockades synergistically inhibited the distant tumor growth, depending on $CD8^+$ as well as NK cells. (A) MM3MG-HER2 cells were injected into both the left leg (1×10^6 cells) and the right flank (5×10^5 cells) of BALB/c mice on day 0. We chose to implant a larger number of cells in the flank, compared with figure 1C, to create a more stringent model. Established leg tumors were treated with M-HIFU on day 7. Anti-PD-L1 antibody (100 µg /100 µL) or isotype control IgG (100 µg /100 µL) was injected intraperitoneally on days 10, 13 and 16. (B) The tumor growth curves of the distant flank tumor are shown. n=10 mice per each group, 40 mice in total. (C,D) On day 18, distant flank tumors (HIFU untreated side) were collected and infiltrating immune cells were analyzed by flow cytometry. n=3 (combination group) or 4 (other groups). (C) The percentages of $CD4^+$, $CD8^+$ and $CD49b^+$ cells in $CD45^+$ cells are shown. (D) The expression of ICOS and Foxp3 on $CD4^+$ cells and the expression of ICOS and granzyme B by $CD8^+$ cells. (E) Mice were treated with the combination of M-HIFU and anti-PD-L1 antibody in the same treatment schedule as figure 4A with or without administration of depleting antibody for $CD4^+$, $CD8a^+$, and NK cells on days 6, 9, 14, and every 5 days until the end of the experiment. (F) The tumor growth curves of the leg tumor (left) and the flank tumor (right) are shown. n=5 mice per each group, 25 mice in total. (B,F) Error bars represent SE. (C,D) Error bars represent SD. *P<0.05, **P<0.01, ***P<0.001, ****P<0.0001. HER2, human ErbB-2; M-HIFU, mechanical high-intensity focused ultrasound; NK, natural killer; PD-1, programmed death-1; PD-L1, programmed cell death ligand 1.

contralateral tumors. A potential criticism is that there are a wide variety of T-HIFU protocols which might induce quite different antitumor effects or antitumor immune responses compared with our T-HIFU technique. Sheybani *et al*[38] recently reported data using a form of T-HIFU (thermal ablative focused ultrasound) to treat poorly immunogenic 4T1 tumors. Although thermal ablation alone had limited impact on the intratumoral accumulation of activated T cells (attributed to the immunosuppressive TME), combination with gemcitabine resulted in enhanced tumor control and improved survival of mice in a CD8 and CD4 T cell-dependent fashion. T-HIFU of BCs in patients was reported to enhance infiltration of immune cells.[22] Recent studies have demonstrated enhanced immunogenicity of BC treated by T-HIFU in combination with systemic ICB or local application of toll-like receptor 9 agonist CpG.[39 40] It is also possible that the timing of immune assays might have affected the outcome of the comparative analysis between the different treatments. For example, T-HIFU-treated tumors could be within the adaptive resistance/wound healing phase at the time of tissue collection in our study. Even taking these into account, we believe that the data of our immune assays, which corresponded well to in vivo antitumor efficacy, indicate the overall capacities of these 2 HIFU modes in the induction of antitumor immunity. More preclinical and clinical studies are necessary to assess

and optimize the antitumor efficacy of HIFU for BC treatment.

Although M-HIFU could significantly inhibit the growth of treated tumors and lengthen the survival of single tumor-bearing mice, the antitumor activity generated against the untreated remote tumors was modest. One explanation we observed was the upregulation of PD-L1 by myeloid cell populations including macrophages in M-HIFU-treated tumors, which may have resulted in the induction of insufficient systemic antitumor immunity. PD-L1 has been shown to exert constitutive negative signals in macrophages and induce an immunosuppressive phenotype.[41] Anti-PD-L1 treatment by itself remodeled the macrophage compartment in tumors toward a more proinflammatory phenotype, mainly through increased IFN-γ levels in TME, resulting in enhanced T-cell activity.[42] In our current study, administration of anti-PD-L1 antibody with M-HIFU enhanced the antitumor efficacy against remote tumors. Importantly, our data suggest that the net effect of combination treatment is a more favorable pattern of T and NK cell attraction and activation not only at the site of the HIFU-treated tumor, but also at distant untreated tumors. Qu and colleagues using a similar mechanical ablative strategy combined with anti-CTLA-4 antibody, reported enhanced systemic antitumor efficacy in murine melanoma and hepatoma models.[43] As described earlier, others have combined HIFU with pathogen-associated molecular patterns, such as CpG, to generate an abscopal effect.[39 44] These data, in conjunction with our demonstration that tumor control is CD8+ T cell dependent, support the contention that HIFU induces antigen-specific CD8+ T-cell responses that can be enhanced by nonspecific immune stimulators.

Despite the substantial antitumor effect of the combination therapy, some distant tumors grew after an initial period of control. We hypothesize that there are two potential explanations for the lack of complete control. First, following tumor apoptosis in response to M-HIFU plus anti-PD-L1, tissue repair within the altered TME might involve macrophage repolarization to M2 as previously observed.[45–47] In the models combining M-HIFU and anti-PD-L1, macrophage genes involved in cell matrix adhesion and extracellular matrix organization, important for wound healing, were upregulated in addition to genes typically associated with the M1 phenotype. However, we have previously observed this phenomenon of increased intratumoral phagocytic macrophages with upregulated gene signatures for wound healing, ECM remodeling, and anti-inflammation in anti-CD47 antibody-treated murine BCs experiencing ongoing tumor regression.[48] Therefore, the tendency to upregulate gene expression consistent with a reparative phenotype may not be detrimental once the initial antitumor immune response is activated by M1 macrophages. Second, intratumoral Treg derived from infiltrating $CD4^+$ T cells[49] might counteract effector T-cell function. Our flow cytometric analysis of M-HIFU-treated tumor demonstrates that the combination strategy increased infiltration of $CD4^+$ T cells including a population with enhanced Foxp3 expression, consistent with Treg cells. The depletion of $CD4^+$ Tregs enhanced the antitumor efficacy of the combination treatment locally and in HIFU-untreated distant tumors.

A final criticism of our observations is that human BC is not traditionally considered an inflamed immunogenic tumor and is less responsive to immunotherapies, such as ICB, compared with other immunogenic solid tumors as melanoma and lung cancer.[50] In this study, to monitor induction of tumor-antigen specific immune response by HIFU treatment, we used the tumor models that were engineered to express OVA, HER2 or HER3 antigen. Forced expression of these foreign antigens would make the tumor cells more immunogenic, unlike human BC cases, and thus we need to carefully interpret the induced antigen-specific immune responses in these models. Importantly, however, in one of our BC models, JC-HER3 tumors were implanted into HER3 transgenic mice that are immune tolerant for HER3 antigen,[28] and we could confirm the induction of anti-HER3 cellular immune responses with significant antitumor efficacy and abscopal effect by M-HIFU treatment. These data suggest that M-HIFU is able to break immune tolerance to self-antigens.

In summary, we demonstrated a beneficial modification of the TME by M-HIFU and enhanced systemic antitumor efficacy by the combination of M-HIFU and anti-PD-L1 antibody, which resulted in significantly stronger growth suppression of distant tumors compared with M-HIFU or anti-PD-L1 monotherapy. To further enhance the antitumor efficacy and eradicate distant tumors by induced antitumor immunity, we are testing clinically applicable strategies to combine with M-HIFU plus anti-PD-L1, such as depletion of Tregs by targeting antibodies and enhancing the M1-biased TME by intratumoral IL-12 gene therapy.[12]

Author affiliations
[1]Department of Surgery, Duke University Medical Center, Durham, North Carolina, USA
[2]Department of Surgical Oncology, Faculty of Medicine, The University of Tokyo Graduate School of Medicine, Bunkyo-ku, Tokyo, Japan
[3]Department of Surgery, Jichi Medical University, Shimotsuke, Tochigi, Japan
[4]Department of Medicine, University of Washington, Seattle, Washington, USA
[5]Department of Medicine, Duke University Medical Center, Durham, North Carolina, USA
[6]Department of Mechanical Engineering and Materials Science, Duke University, Durham, North Carolina, USA

Twitter Pankaj Agarwal @pagarwal14

Contributors All the coauthors contributed to the study and the writing/editing of the manuscript. Concept and experimental design: TO, HKL and PZ. Acquisition of data: SA, HN, YI, KK, C-XL, XY and TW. Data analysis and interpretation: SA, EJC, PA, JS and TO. Writing and review of the manuscript: SA, WG, MAM and TO. Study supervision: PZ, HKL and TO. TO is a guarantor for this study and publication.

Funding This research was partly supported by MEDx funding of Duke University (2016).

Competing interests None declared.

Patient consent for publication Not applicable.

Ethics approval All in vivo experiments were conducted in accordance with the Institutional Animal Care and Use Committee of Duke University Medical Center (protocols: A274-15-10 and A223-18-09). Protocols were prepared and approved before the study. Animals were maintained in a barrier facility, under pathogen-free conditions according to National Institutes of Health guidelines.

Provenance and peer review Not commissioned; externally peer reviewed.

Data availability statement Data are available upon reasonable request. Tumor growth data are uploaded as supplementary information. All other data are available upon reasonable request to the correspondence author.

ORCID iDs
Erika J Crosby http://orcid.org/0000-0002-4872-6711
Chaitanya R Acharya http://orcid.org/0000-0001-7149-1749
Herbert Kim Lyerly http://orcid.org/0000-0002-0063-4770
Takuya Osada http://orcid.org/0000-0003-1424-5001

REFERENCES

1 Chikarmane SA, Tirumani SH, Howard SA, *et al*. Metastatic patterns of breast cancer subtypes: what radiologists should know in the era of personalized cancer medicine. *Clin Radiol* 2015;70:1–10.
2 Gong Y, Liu Y-R, Ji P, *et al*. Impact of molecular subtypes on metastatic breast cancer patients: a SEER population-based study. *Sci Rep* 2017;7:45411.
3 Xiao W, Zheng S, Yang A, *et al*. Breast cancer subtypes and the risk of distant metastasis at initial diagnosis: a population-based study. *Cancer Manag Res* 2018;10:5329–38.
4 Adams S, Schmid P, Rugo HS, *et al*. Pembrolizumab monotherapy for previously treated metastatic triple-negative breast cancer: cohort a of the phase II KEYNOTE-086 study. *Ann Oncol* 2019;30:397–404.
5 Emens LA, Cruz C, Eder JP, *et al*. Long-term clinical outcomes and biomarker analyses of Atezolizumab therapy for patients with metastatic triple-negative breast cancer: a phase 1 study. *JAMA Oncol* 2019;5:74–82.
6 Zhou H, Liu L, Lee K, *et al*. Lung tumorigenesis associated with erb-B-2 and erb-B-3 overexpression in human erb-B-3 transgenic mice is enhanced by methylnitrosourea. *Oncogene* 2002;21:8732–40.
7 Chung W, Eum HH, Lee H-O, *et al*. Single-cell RNA-seq enables comprehensive tumour and immune cell profiling in primary breast cancer. *Nat Commun* 2017;8:15081.
8 Patel AP, Tirosh I, Trombetta JJ, *et al*. Single-cell RNA-seq highlights intratumoral heterogeneity in primary glioblastoma. *Science* 2014;344:1396–401.
9 Wang N, Wang S, Wang X, *et al*. Research trends in pharmacological modulation of tumor-associated macrophages. *Clin Transl Med* 2021;11:e288.
10 He K, Jia S, Lou Y, *et al*. Cryo-thermal therapy induces macrophage polarization for durable anti-tumor immunity. *Cell Death Dis* 2019;10:216.
11 Li M, Kirtane AR, Kiyokawa J. Local targeting of NAD+ salvage pathway alters the immune tumor microenvironment and enhances checkpoint immunotherapy in glioblastoma. *Cancer Res* 2020;80:22:5024–34.
12 Telli ML, Nagata H, Wapnir I, *et al*. Intratumoral plasmid IL12 expands $CD8^+$ T cells and induces a CXCR3 gene signature in triple-negative breast tumors that sensitizes patients to anti-PD-1 therapy. *Clin Cancer Res* 2021;27:2481–93.
13 Melero I, Castanon E, Alvarez M, *et al*. Intratumoural administration and tumour tissue targeting of cancer immunotherapies. *Nat Rev Clin Oncol* 2021;18:558–76.
14 Najafi M, Hashemi Goradel N, Farhood B, *et al*. Macrophage polarity in cancer: a review. *J Cell Biochem* 2019;120:2756–65.
15 Tariq M, Zhang J, Liang G, *et al*. Macrophage polarization: anti-cancer strategies to target tumor-associated macrophage in breast cancer. *J Cell Biochem* 2017;118:2484–501.
16 Xiao Y, Ma D, Zhao S, *et al*. Multi-omics profiling reveals distinct microenvironment characterization and suggests immune escape mechanisms of triple-negative breast cancer. *Clin Cancer Res* 2019;25:5002–14.
17 Cassetta L, Fragkogianni S, Sims AH, *et al*. Human tumor-associated macrophage and monocyte transcriptional landscapes reveal cancer-specific reprogramming, biomarkers, and therapeutic targets. *Cancer Cell* 2019;35:588–602.
18 Kennedy JE. High-intensity focused ultrasound in the treatment of solid tumours. *Nat Rev Cancer* 2005;5:321–7.
19 Mauri G, Sconfienza LM, Pescatori LC, *et al*. Technical success, technique efficacy and complications of minimally-invasive imaging-guided percutaneous ablation procedures of breast cancer: a systematic review and meta-analysis. *Eur Radiol* 2017;27:3199–210.
20 den Brok MHMGM, Sutmuller RPM, van der Voort R, *et al*. In situ tumor ablation creates an antigen source for the generation of antitumor immunity. *Cancer Res* 2004;64:4024–9.
21 Chida S, Okada K, Suzuki N, *et al*. Infiltration by macrophages and lymphocytes in transplantable mouse sarcoma after irradiation with high-intensity focused ultrasound. *Anticancer Res* 2009;29:3877–82.
22 Lu P, Zhu X-Q, Xu Z-L, *et al*. Increased infiltration of activated tumor-infiltrating lymphocytes after high intensity focused ultrasound ablation of human breast cancer. *Surgery* 2009;145:286–93.
23 Wu F, Wang Z-B, Cao Y-D, *et al*. A randomised clinical trial of high-intensity focused ultrasound ablation for the treatment of patients with localised breast cancer. *Br J Cancer* 2003;89:2227–33.
24 Sabel MS. Cryo-immunology: a review of the literature and proposed mechanisms for stimulatory versus suppressive immune responses. *Cryobiology* 2009;58:1–11.
25 Hu Z, Yang XY, Liu Y, *et al*. Release of endogenous danger signals from HIFU-treated tumor cells and their stimulatory effects on APCs. *Biochem Biophys Res Commun* 2005;335:124–31.
26 Xia J-Z, Xie F-L, Ran L-F, *et al*. High-intensity focused ultrasound tumor ablation activates autologous tumor-specific cytotoxic T lymphocytes. *Ultrasound Med Biol* 2012;38:1363–71.
27 Osada T, Kaneko K, Gwin WR, *et al*. *In Vivo* detection of HSP90 identifies breast cancers with aggressive behavior. *Clin Cancer Res* 2017;23:7531–42.
28 Osada T, Morse MA, Hobeika A, *et al*. Vaccination targeting human HER3 alters the phenotype of infiltrating T cells and responses to immune checkpoint inhibition. *Oncoimmunology* 2017;6:e1315495.
29 Kershaw MH, Jackson JT, Haynes NM, *et al*. Gene-engineered T cells as a superior adjuvant therapy for metastatic cancer. *J Immunol* 2004;173:2143–50.
30 Hu Z, Yang XY, Liu Y, *et al*. Investigation of HIFU-induced anti-tumor immunity in a murine tumor model. *J Transl Med* 2007;5:34.
31 Khokhlova TD, Haider YA, Maxwell AD, *et al*. Dependence of boiling histotripsy treatment efficiency on HIFU frequency and focal pressure levels. *Ultrasound Med Biol* 2017;43:1975–85.
32 Yuan F, Yang C, Zhong P. Cell membrane deformation and bioeffects produced by tandem bubble-induced jetting flow. *Proc Natl Acad Sci U S A* 2015;112:E7039–47.
33 Piechocki MP, Ho Y-S, Pilon S, *et al*. Human ErbB-2 (HER-2) transgenic mice: a model system for testing HER-2 based vaccines. *J Immunol* 2003;171:5787–94.
34 Orecchioni M, Ghosheh Y, Pramod AB. Macrophage polarization: different gene signatures in M1(LPS+) vs. classically and M2(LPS-) vs. alternatively activated macrophages. Front Immunol. 2019 May 24;10:1084. *Front Immunol* 2020;11:234.
35 Murray PJ, Allen JE, Biswas SK, *et al*. Macrophage activation and polarization: nomenclature and experimental guidelines. *Immunity* 2014;41:14–20.
36 Jablonski KA, Amici SA, Webb LM, *et al*. Novel markers to delineate murine M1 and M2 macrophages. *PLoS One* 2015;10:e0145342.
37 Pitt JM, Marabelle A, Eggermont A, *et al*. Targeting the tumor microenvironment: removing obstruction to anticancer immune responses and immunotherapy. *Ann Oncol* 2016;27:1482–92.
38 Sheybani ND, Witter AR, Thim EA, *et al*. Combination of thermally ablative focused ultrasound with gemcitabine controls breast cancer via adaptive immunity. *J Immunother Cancer* 2020;8:e001008.
39 Silvestrini MT, Ingham ES, Mahakian LM, *et al*. Priming is key to effective incorporation of image-guided thermal ablation into immunotherapy protocols. *JCI Insight* 2017;2:e90521.
40 Fite BZ, Wang J, Kare AJ, *et al*. Immune modulation resulting from MR-guided high intensity focused ultrasound in a model of murine breast cancer. *Sci Rep* 2021;11:927.

41 Hartley GP, Chow L, Ammons DT, *et al*. Programmed cell death ligand 1 (PD-L1) signaling regulates macrophage proliferation and activation. *Cancer Immunol Res* 2018;6:1260–73.
42 Xiong H, Mittman S, Rodriguez R, *et al*. Anti-PD-L1 treatment results in functional remodeling of the macrophage compartment. *Cancer Res* 2019;79:1493–506.
43 Qu S, Worlikar T, Felsted AE, *et al*. Non-thermal histotripsy tumor ablation promotes abscopal immune responses that enhance cancer immunotherapy. *J Immunother Cancer* 2020;8:e000200.
44 van den Bijgaart RJE, Eikelenboom DC, Hoogenboom M, *et al*. Thermal and mechanical high-intensity focused ultrasound: perspectives on tumor ablation, immune effects and combination strategies. *Cancer Immunol Immunother* 2017;66:247–58.
45 Fadok VA, Bratton DL, Konowal A, *et al*. Macrophages that have ingested apoptotic cells in vitro inhibit proinflammatory cytokine production through autocrine/paracrine mechanisms involving TGF-beta, PGE2, and PAF. *J Clin Invest* 1998;101:890–8.
46 Lech M, Anders H-J. Macrophages and fibrosis: how resident and infiltrating mononuclear phagocytes orchestrate all phases of tissue injury and repair. *Biochim Biophys Acta* 2013;1832:989–97.
47 Minutti CM, Knipper JA, Allen JE, *et al*. Tissue-specific contribution of macrophages to wound healing. *Semin Cell Dev Biol* 2017;61:3–11.
48 Tsao L-C, Crosby EJ, Trotter TN, *et al*. CD47 blockade augmentation of trastuzumab antitumor efficacy dependent on antibody-dependent cellular phagocytosis. *JCI Insight* 2019;4:e131882.
49 Su S, Liao J, Liu J, *et al*. Blocking the recruitment of naive $CD4^+$ T cells reverses immunosuppression in breast cancer. *Cell Res* 2017;27:461–82.
50 Alexandrov LB, Nik-Zainal S, Wedge DC, *et al*. Signatures of mutational processes in human cancer. *Nature* 2013;500:415–21.